The Astrophysical Journal Letters, 898:L5 (6pp), 2020 July 20 https://doi.org/10.3847/2041-8213/aba262

On the Distance of SGR 1935+2154 Associated with FRB 200428 and Hosted in SNR G57.2+0.8

Shu-Qing Zhong[1,2], Zi-Gao Dai[1,2], Hai-Ming Zhang[1,2], and Can-Min Deng[3,4]
[1] School of Astronomy and Space Science, Nanjing University, Nanjing 210093, People's Republic of China; dzg@nju.edu.cn
[2] Key Laboratory of Modern Astronomy and Astrophysics (Nanjing University), Ministry of Education, Nanjing 210093, People's Republic of China
[3] Department of Astronomy, School of Physical Sciences, University of Science and Technology of China, Hefei, Anhui 230026, People's Republic of China
[4] CAS Key Laboratory for Research in Galaxies and Cosmology, Department of Astronomy, University of Science and Technology of China, Hefei 230026, Anhui, People's Republic of China
Received 2020 May 22; revised 2020 June 27; accepted 2020 July 2; published 2020 July 17

Abstract

Owing to the detection of an extremely bright fast radio burst (FRB) 200428 associated with a hard X-ray counterpart from the magnetar soft gamma-ray repeater (SGR) 1935+2154, the distance of SGR 1935+2154 potentially hosted in the supernova remnant (SNR) G57.2+0.8 can be revisited. Under the assumption that the SGR and the SNR are physically related, in this Letter, by investigating the dispersion measure (DM) of the FRB contributed by the foreground medium of our Galaxy and the local environments and combining other observational constraints, we find that the distance of SGR 1935+2154 turns out to be 9.0 ± 2.5 kpc and the SNR radius falls into 10–18 pc since the local DM contribution is as low as 0–18 pc cm^{-3}. These results are basically consistent with previous studies. In addition, an estimate for the Faraday rotation measure of the SGR and SNR is also carried out.

Unified Astronomy Thesaurus concepts: Magnetars (992); Soft gamma-ray repeaters (1471); Radio transient sources (2008); Radio bursts (1339); X-ray bursts (1814); Supernova remnants (1667)

1. Introduction

Very recently, an extremely bright millisecond-timescale radio burst from the Galactic magnetar SGR 1935+2154 was reported by The CHIME/FRB Collaboration et al. (2020) and Bochenek et al. (2019). More excitingly, its associated X-ray burst counterpart was also detected by Insight-HXMT (Li et al. 2020; Zhang et al. 2020b, 2020c, 2020d), AGILE (Tavani et al. 2020), INTEGRAL (Mereghetti et al. 2020), and Konus–Wind (Ridnaia et al. 2020) telescopes. Additionally, a subsequent highly polarized transient pulsating radio burst was detected by the FAST radio telescope with Faraday rotation measure (RM) $+112.3$ rad m^{-2} (Zhang et al. 2020a), consistent with RM $= +116 \pm 6$ rad m^{-2} of FRB 200428 (The CHIME/FRB Collaboration et al. 2020). From the previous investigations about the magnetar SGR 1935+2154, we know that it has a spin period $P \simeq 3.24$ s, a spin-down rate $\dot{P} \simeq 1.43 \times 10^{-11}$ s s^{-1}, a surface dipole magnetic field strength $B_{\rm p} \simeq 2.2 \times 10^{14}$ G, an age $t \sim 3.6$ kyr, and a spin-down luminosity $L_{\rm sd} \sim 1.7 \times 10^{34}$ erg s^{-1} (Israel et al. 2016), hosted in the Galactic supernova remnant (SNR) G57.2+0.8 with a high probability (Gaensler 2014).

In the literature, however, the distance of SNR G57.2+0.8 has a large range and remains highly debated even though various methods have been used, e.g., the statistical radio surface-brightness-to-diameter relation (~9.1 kpc, Pavlović et al. 2013), the empirical relation between the H I column density $N_{\rm H}$ and the dispersion measure (DM) (11.7 ± 2.8 kpc, Surnis et al. 2016), and the local standard of rest (LSR) velocity measure via the HI absorption feature (12.5 ± 1.5 kpc, Kothes et al. 2018; 4.5–9.0 kpc, Ranasinghe et al. 2018), or via CO gas toward the SNR (6.6 ± 0.7 kpc, Zhou et al. 2020). For SGR 1935+2154, Kozlova et al. (2016) gave an upper limit <10 kpc through the scattered correlation between the squares of the radii of the emitting areas and the corresponding blackbody temperatures, and Mereghetti et al. (2020) obtained 2.2–7.1 kpc through the observation of the bright dust-scattering X-ray ring. Note that the methods tracing the SNR are radio-based only and those tracing the SGR are X-ray-based only. Due to the position of the SGR at the geometric center of the SNR in a relatively uncrowded region of the Galactic plane (Gaensler 2014), to the distance estimates and approximate ages inferred for the SGR and the SNR, it is believed that they are likely physically related (Kothes et al. 2018). Moreover, the relatively small age (3.6 kyr) of the SGR supports that its SNR should be visible (Zhou et al. 2020). All these pieces of evidence strongly suggest a likely association between the SGR and the SNR.

In this Letter, we therefore assume that SGR 1935+2154 is indeed associated with SNR G57.2+0.8 and the SNR has the same age as the SGR, and we then use DM by combining with other observational constraints to estimate the distance of the SGR in Section 2. Our results are displayed in Section 3. A discussion on the RM estimate is arranged in Section 4, and conclusions are drawn in Section 5.

2. DM Estimate

The CHIME/FRB Collaboration et al. (2020) and Bochenek et al. (2019) reported that FRB 200428 has an observed DM$_{\rm obs} = 332.7$ pc cm^{-3}. The DM$_{\rm obs}$ is mainly contributed by the foreground interstellar medium (ISM) in our Galaxy (DM$_{\rm Gal}$), the magnetar wind nebula (DM$_{\rm MWN}$), and the SNR (DM$_{\rm SNR}$), that is,

$$\mathrm{DM_{obs}} = \mathrm{DM_{Gal}} + \mathrm{DM_{MWN}} + \mathrm{DM_{SNR}}, \quad (1)$$

where the foreground DM of our Galaxy is

$$\mathrm{DM_{Gal}} = \int_0^D n_e(l)\,dl, \quad (2)$$

related to the distance D of SGR 1935+2154 via the Galactic electron density (n_e) distribution NE2001 (Cordes & Lazio 2002, 2003) or YMW16[5] (Yao et al. 2017).

The $\mathrm{DM_{MWN}}$ is primarily attributed to the O-mode wave and may be given by (e.g., Yu 2014; Cao et al. 2017; Yang & Zhang 2017)

$$\mathrm{DM_{MWN}} \simeq 0.082\ \mathrm{pc\ cm^{-3}}\ \mu_{\pm,4}^{2/3} B_{\mathrm{p},14}^{4/3} P_0^{-11/3}, \tag{3}$$

where $\mu_\pm = 10^4 \mu_{\pm,4}$ is the multiplicity parameter of the electron–positron pairs, $B_\mathrm{p} = 10^{14} B_{\mathrm{p},14}$ G and $P = 10^0 P_0$ s are the dipole magnetic field and the rotation period of the magnetar, respectively.

In regards to the $\mathrm{DM_{SNR}}$, it depends on ambient medium: constant density ISM or wind environment. So we consider the DM contribution by the SNR in two different scenarios as follows.

2.1. Constant ISM

It is widely accepted that an SNR has three phases after a supernova (SN) explosion in the constant ISM scenario: (a) the free-expansion phase, (b) the Sedov–Taylor phase, and (c) the snowplow phase. Because SNR G57.2+0.8 has possibly reached the end of the Sedov–Taylor phase or entered the snowplow phase due to the nondetection of X-ray emission (Kothes et al. 2018; Zhou et al. 2020), the $\mathrm{DM_{SNR}}$ from the ionized medium (including shocked SN ejecta and shocked swept ambient medium[6]), can be estimated by

$$\mathrm{DM_{SNR}} \simeq \begin{cases} 34\ \mathrm{pc\ cm^{-3}}\ t_2^{2/5} E_{51}^{1/5} n_2^{4/5}, & t < t_\mathrm{SP} \\ 81\ \mathrm{pc\ cm^{-3}}\ t_3^{2/7} E_{51}^{0.225} n_2^{0.737}, & t > t_\mathrm{SP} \end{cases} \tag{4}$$

during the Sedov–Taylor and snowplow phases (e.g., Yang & Zhang 2017; Piro & Gaensler 2018), where $t = 10^i t_i$ yr is the age of the SNR, $E = 10^{51} E_{51}$ erg is the energy of the SN explosion, and $n = 10^2 n_2$ cm^{-3} is the number density of a uniform ISM, as well as the snowplow time $t_\mathrm{SP} \simeq 3920\ \mathrm{yr}\ E_{51}^{0.22} n_2^{-0.55}$ (e.g., Draine 2011). The corresponding SNR radius can be written as (e.g., Taylor 1950; Sedov 1959; Draine 2011; Yang & Zhang 2017)

$$R_\mathrm{SNR} \simeq \begin{cases} 0.84\ \mathrm{pc}\ t_2^{2/5} E_{51}^{1/5} n_2^{-1/5}, & t < t_\mathrm{SP} \\ 2.44\ \mathrm{pc}\ t_3^{2/7} E_{51}^{0.225} n_2^{-0.263}, & t > t_\mathrm{SP} \end{cases}, \tag{5}$$

where we have used the Sedov–Taylor radius independent of the mass of the SN ejecta as the SNR radius (Yang & Zhang 2017) rather than the blastwave radius depending on the mass of the SN ejecta (Piro & Gaensler 2018), because the Sedov–Taylor radius can be a good representation of the SNR radius when the SNR has been well past the free-expansion phase.

[5] Throughout the paper, we adopt the Galactic electron model YMW16 encoded in the pygedm package of Python because this model is believed to give more reliable estimates than NE2001 in general (see Table 6 of Yao et al. 2017).

[6] We assume the swept ambient medium is fully ionized in order to acquire an upper limit of the $\mathrm{DM_{SNR}}$. Meanwhile, we neglect the unshocked ambient medium upstream of the shock since it is neutral-hydrogen-dominated, as done in Piro & Gaensler (2018).

2.2. Wind Environment

In a wind environment, the SNR evolution has two phases: the early ejecta-dominated phase and the very late wind-dominated phase, based on Piro & Gaensler (2018). During these phases, the $\mathrm{DM_{SNR}}$ is calculated by (see Table 2 of Piro & Gaensler 2018)

$$\mathrm{DM_{SNR}} \simeq \begin{cases} 13\ \mathrm{pc\ cm^{-3}}\ \mu_e^{-1} t_2^{-3/2} E_{51}^{-3/4} M_1^{5/4} K_{13}^{1/2}, \\ t < t_\mathrm{ch} \\ 0.088\ \mathrm{pc\ cm^{-3}}\ \mu_e^{-1} t_3^{-2/3} E_{51}^{-1/3} K_{13}^{4/3}, \\ t > t_\mathrm{ch} \end{cases} \tag{6}$$

where μ_e is the mean molecular weight per electron, $M = M_1 \times 1 M_\odot$ is the mass of the SN ejecta, $K = 5.1 \times 10^{13}\ \mathrm{g\ cm^{-1}}\ \dot{M}_{-5} v_6^{-1}$ (here the mass-loss rate $\dot{M}_{-5} = 10^{-5} M_\odot\ \mathrm{yr^{-1}}$ and the wind velocity $v_6 = v_w / 10^6\ \mathrm{cm\ s^{-1}}$), and the characteristic time $t_\mathrm{ch} = 1.9 \times 10^3\ \mathrm{yr}\ E_{51}^{-1/2} M_1^{3/2} K_{13}^{-1}$ separating these phases. This characteristic time corresponds to a radius $R_\mathrm{ch} = 16.8\ \mathrm{pc}\ M_1 K_{13}^{-1}$. Please note that the SNR radius deemed as the blastwave radius can be linked to R_ch and t_ch through the analytic functions (see Table 2 of Piro & Gaensler 2018)

$$R_\mathrm{SNR} \simeq \begin{cases} 1.79 R_\mathrm{ch} (t/t_\mathrm{ch}) [1 + 0.33 (t/t_\mathrm{ch})^{1/2}]^{-2}, \\ t < t_\mathrm{ch} \\ [1.11 (t/t_\mathrm{ch}) - 0.11]^{2/3} R_\mathrm{ch}, \\ t > t_\mathrm{ch}. \end{cases} \tag{7}$$

3. DM Results

A useful observational constraint for SNR G57.2+0.8 is that it is an almost circular source with an average diameter of about 10′, i.e., radius $\theta_\mathrm{r} \approx 5\farcm5$ (Kothes et al. 2018), which is relevant to the SNR radius via the distance of SGR 1935+2154

$$D = \frac{R_\mathrm{SNR}}{\theta_\mathrm{r}}. \tag{8}$$

Likewise, the observational constraints for $\mathrm{DM_{obs}}$, t, B_p, and P are also known. Through the calculation of Equation (3), we find that the value of $\mathrm{DM_{MWN}}$ is far smaller than 1 pc cm^{-3} even if $\mu_\pm$ is very large like 10^6, so we safely ignore this term in Equation (1) for subsequent calculations.

In the ISM scenario for the SNR, utilizing Equations (1), (2), (4), (5), and (8), one gets a power-law relation with an index 1.0 between the explosion energy E and the ambient medium density n (using parameter values $\theta_\mathrm{r} \approx 5\farcm5$, $\mathrm{DM_{obs}} = 332.7\ \mathrm{pc\ cm^{-3}}$, and $t = 3.6$ kyr), as illustrated in the top panel of Figure 1. Furthermore, it is obvious that the ambient medium density has a relatively small value, i.e., <5 cm^{-3}, within a typical explosion energy ranging from several 10^{49} erg to several 10^{51} erg (e.g., Pejcha & Prieto 2015; Lyman et al. 2016). Meanwhile, one can also acquire a distance distribution $D \simeq 6.5$–11.5 kpc with a mean value 9.0 kpc (so the SNR radius $R_\mathrm{SNR} \simeq 10$–18 pc), and a DM distribution of the SNR $\mathrm{DM_{SNR}} \simeq 0$–$18\ \mathrm{pc\ cm^{-3}}$ illustrating in the middle and bottom panels of Figure 1. Obviously, the $\mathrm{DM_{SNR}}$ is very low, compared with the Galactic contribution $\mathrm{DM_{Cal}}$. Note that we have considered the uncertainty for the distance estimate via YMW16 model throughout the numerical calculations since it is the main uncertainty. As shown in Table 4 of Yao et al. (2017), the direction of SGR 1935+2154 is closest to

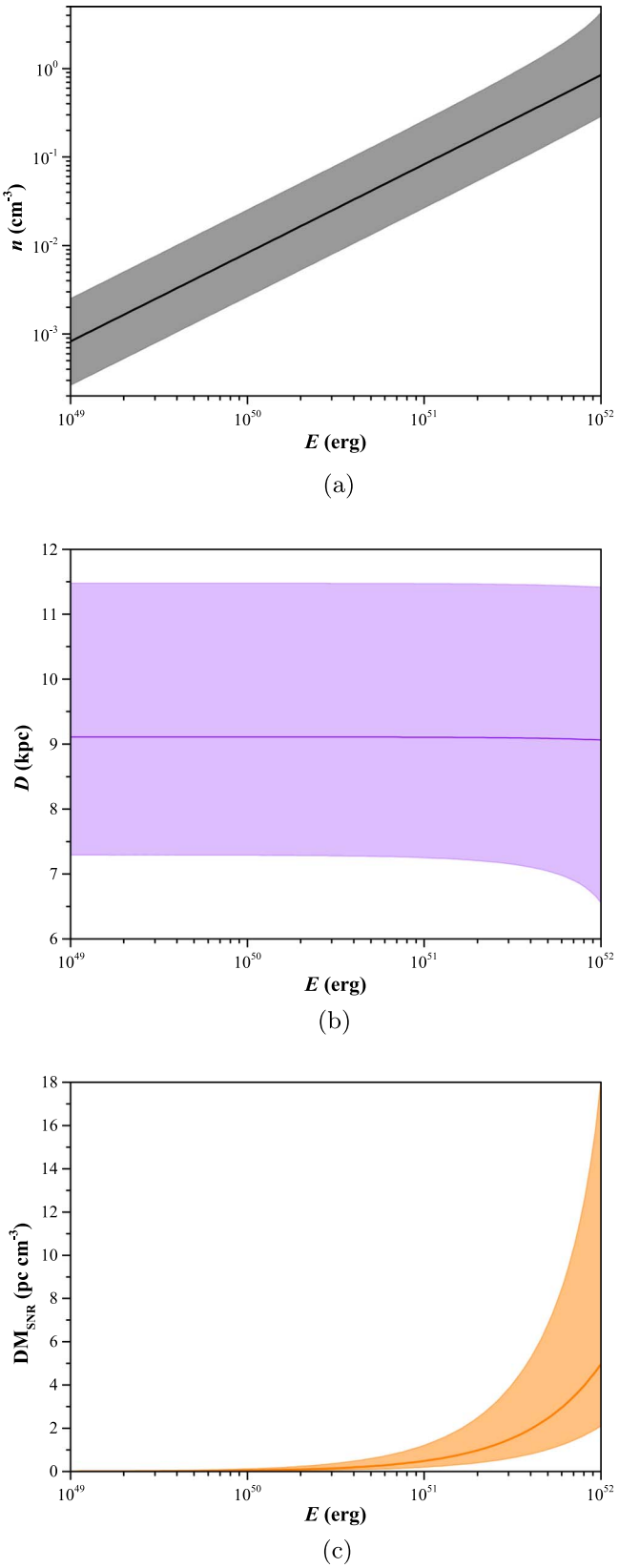

Figure 1. In a constant ISM for the SNR: (a) ambient medium density n as a power-law function of energy of SN explosion E (top panel); (b) the distance D of SGR 1935+2154 is varied with energy of SN explosion E (middle panel); (c) $\mathrm{DM_{SNR}}$ vs. explosion energy E (bottom panel). The lines in the three panels represent the results without considering the uncertainty for the distance estimate via the YMW16 model.

that of the pulsar J1932+2220 with a relative uncertainty $D_{\rm err} \sim 26\%$ for the distance estimate, thus the distance of SGR 1935+2154 could also have a relative uncertainty ~26%. The lines in Figure 1 represent the numerical results without considering the uncertainty for the distance. In reality, it is easy to roughly check these numerical results such as $E \propto n$ via $\mathrm{DM_{obs}} \propto \mathrm{DM_{Gal}} \propto D \propto R_{\rm SNR} \propto E^{1/5} n^{-1/5}$ for $t < t_{\rm SP}$ when $\mathrm{DM_{obs}}$ is dominated by $\mathrm{DM_{Gal}}$.

For a wind environment toward the SNR, employing Equations (1), (2), (6),[7] (7), and (8), one obtains a relation between the explosion energy E and the parameter K for $M = 2\,M_\odot$ (stripped-envelope SNe) and $M = 10\,M_\odot$ (red supergiant progenitors), as shown in the top panel of Figure 2. The parameter K declines sharply when the explosion energy $E < 6 \times 10^{50}$ erg ($E < 3 \times 10^{51}$ erg) for $M = 2M_\odot$ ($M = 10M_\odot$), so we calculate the numerical results by only considering the explosion energy $E > 6 \times 10^{50}$ erg ($E > 3 \times 10^{51}$ erg) for $M = 2M_\odot$ ($M = 10M_\odot$). The remaining panels of Figure 2 show that the distance spans $D \simeq 6.5$–11.5 kpc and the DM contribution of the SNR occupies $\mathrm{DM_{SNR}} \simeq 0$–$18$ pc cm^{-3} for both $M = 2M_\odot$ and $M = 10M_\odot$. These results are in good agreement with those in the ISM scenario.

In summary, our results generally agree with those in the previous studies by Pavlović et al. (2013), Surnis et al. (2016), Kothes et al. (2018), Ranasinghe et al. (2018), and Zhou et al. (2020) for SNR G57.2+0.8, and Kozlova et al. (2016) and Mereghetti et al. (2020) for SGR 1935+2154. The methods in Pavlović et al. (2013), Surnis et al. (2016), and Kozlova et al. (2016) are empirical and statistical, with intrinsic large scatter. The methods in Kothes et al. (2018), Ranasinghe et al. (2018), and Zhou et al. (2020) seem to be relevant to direct measurements and their uncertainties mainly stem from the LSR velocity measure and the rotation curve of the Galaxy. While the uncertainties in the method of Mereghetti et al. (2020) may result mostly from the determination of the dust layer and the dust-scattering distance. In comparison, the distance estimate from DM in this Letter is assumption-dependent and model-dependent, though, the results are not variable for different ambient environments. The uncertainty in this method primarily originates from the Galactic electron density distribution of the YMW16 model, i.e., leading to a relative uncertainty $D_{\rm err} \sim 26\%$ for the distance in the direction of SGR 1935+2154.

4. RM Estimate

Similar to the DM estimate, the observed $\mathrm{RM_{obs}}$ should also have three parts: the foreground $\mathrm{RM_{Gal}}$ due to the Galactic ISM and permeating magnetic fields, the $\mathrm{RM_{MWN}}$ contributed by the magnetar wind nebula, and the $\mathrm{RM_{SNR}}$ resulting from the SNR, that is,

$$\mathrm{RM_{obs}} = \mathrm{RM_{Gal}} + \mathrm{RM_{MWN}} + \mathrm{RM_{SNR}}. \quad (9)$$

(1) The first part $\mathrm{RM_{Gal}}$ can be expressed as

$$\mathrm{RM_{Gal}[rad\ m^{-2}]} = 0.81 \int_0^D n_{\rm e}[\mathrm{cm^{-3}}] B_\parallel [\mu G]\, dl\,[\mathrm{pc}] \quad (10)$$

[7] Adopting $\mu_e = 1$. The values of μ_e in a reasonable range cannot significantly influence the final results.

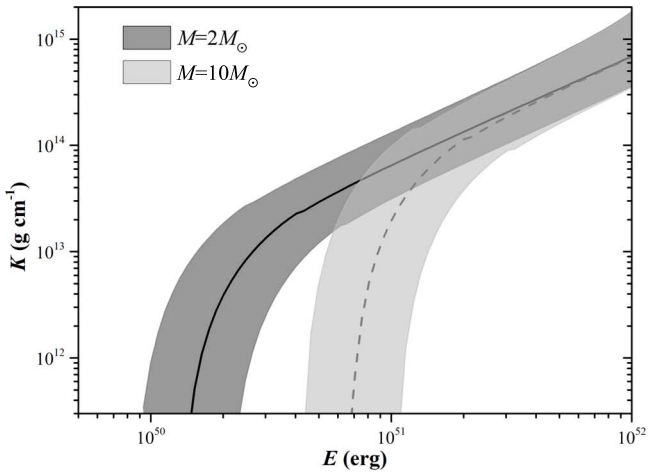

(a)

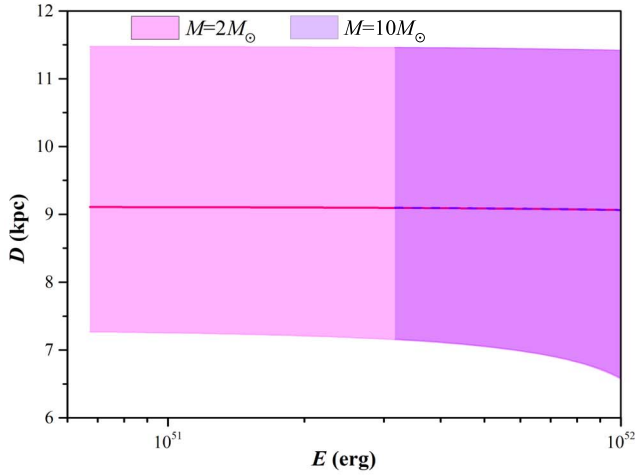

(b)

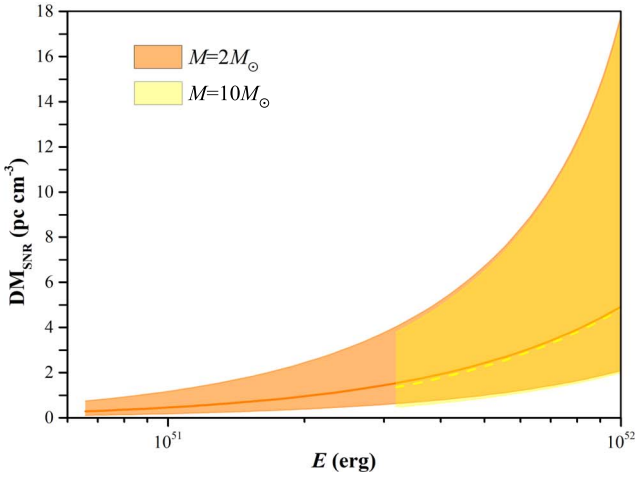

(c)

Figure 2. In a wind environment for the SNR: (a) the parameter $K = 5.1 \times 10^{13}\ \mathrm{g\ cm^{-1}}\ \dot{M}_{-5} v_6^{-1}$ as a function of energy of SN explosion E (top panel); (b) same as the middle panel of Figure 1 (middle panel); (c) same as the bottom panel of Figure 1 (bottom panel). The lines are also the same as those in Figure 1.

where $B_\parallel$ is the component of the Galactic magnetic field (GMF) parallel to the line of sight. RM is positive when the magnetic field points toward us. There is a general model of the GMF consisting of two different components: a disk field and a halo field (Prouza & Šmída 2003; Sun et al. 2008). The widely used disk field is the logarithmic spiral disk GMF model, which has two versions: the axisymmetric disk field (ASS model) and the bisymmetric disk field (BSS model; please see, e.g., Simard-Normandin & Kronberg 1980; Han & Qiao 1994; Stanev 1997; Tinyakov & Tkachev 2002). To estimate the $\mathrm{RM_{Gal}}$, we consider the disk field with an ASS or BSS form and halo field with a basic form (Prouza & Šmída 2003; Sun et al. 2008; Jansson et al. 2009; Sun & Reich 2010; Pshirkov et al. 2011) as done in Lin & Dai (2016), combining with the Galactic free electron distribution n_e in Yao et al. (2017) and the distance from above the DM estimate. However, the $\mathrm{RM_{Gal}}$ has very different values in different models or in the same models but with different parameters, from a few negative hundred to a few hundred rad $\mathrm{m^{-2}}$ within a distance range of $D \simeq 6.5$–11.5 kpc, e.g., ∼470–750 rad $\mathrm{m^{-2}}$ for ASS+halo and ∼50–320 rad $\mathrm{m^{-2}}$ for BSS+halo in Pshirkov et al. (2011), and ∼−220–40 rad $\mathrm{m^{-2}}$ for ASS+halo in Sun et al. (2008). As a result, it cannot be well evaluated by the GMF models. Nevertheless, Kothes et al. (2018) found that the foreground $\mathrm{RM} = +223 \pm 2\ \mathrm{rad\ m^{-2}}$ for SNR G57.2+0.8 via the polarized intensity maps.

(2) The second part $\mathrm{RM_{MWN}}$ arises from the magnetar wind nebula due to the magnetar spin-down energy release. The magnetic field of the nebula at time t can be crudely estimated by (Metzger et al. 2017)

$$B_{\rm n} \simeq \left(\frac{6\epsilon_B L_{\rm sd} t}{R_{\rm n}^3}\right)^{1/2}, \tag{11}$$

where ϵ_B is the ratio of the magnetic energy to the shock energy. Assuming $R_{\rm n} \sim (0.01\text{–}0.1) R_{\rm SNR} \simeq$ 0.1–2 pc, and giving $\epsilon_B \sim 0.1$, $L_{\rm sd} \sim 1.7 \times 10^{34}\ \mathrm{erg\ s^{-1}}$, and $t \sim 3.6$ kyr, one would get $B_{\rm n} \sim 0.5$–$100\ \mu$G. In this case, a very low $\mathrm{RM_{MWN}} \simeq 0.81\ \mathrm{rad\ m^{-2}}\ \frac{\mathrm{DM_{MWN}}}{\mathrm{pc\ cm^{-3}}} \frac{B_{\rm n}}{\mu\mathrm{G}} \sim 0.005$–$0.3\ \mathrm{rad\ m^{-2}}$ is acquired through Equation (3). Although some parameters are uncertain, the $\mathrm{RM_{MWN}}$ should be low if they fall into reasonable ranges.

(3) Akin to the $\mathrm{DM_{SNR}}$ estimate, $\mathrm{RM_{SNR}}$ in different surrounding environments should have different evolutions.

ISM Scenario. In the snowplow phase, the SNR velocity is (Yang & Zhang 2017)

$$v_{\rm SP} = 690\ \mathrm{km\ s^{-1}}\ t_3^{-5/7} E_{51}^{0.445} n_2^{-0.813}, \tag{12}$$

so that the magnetic field generated in the shocked ISM is estimated by (Piro & Gaensler 2018)

$$\begin{aligned} B_{\rm ISM} &\approx (16\pi\epsilon m_p n)^{1/2} v_{\rm SP} \\ &\approx 2.02 \times 10^3\ \mu\mathrm{G}\ \epsilon_{-1}^{1/2} t_3^{-5/7} E_{51}^{0.445} n_2^{-0.313}, \end{aligned} \tag{13}$$

where $\epsilon = 10^{-1}\epsilon_{-1}$ is the ratio of the magnetic energy to the shock energy. Hence, the $\mathrm{RM_{SNR}}$ in the snowplow phase ($t > t_{\rm SP}$) deduced from Equations (4) and (13) can be written

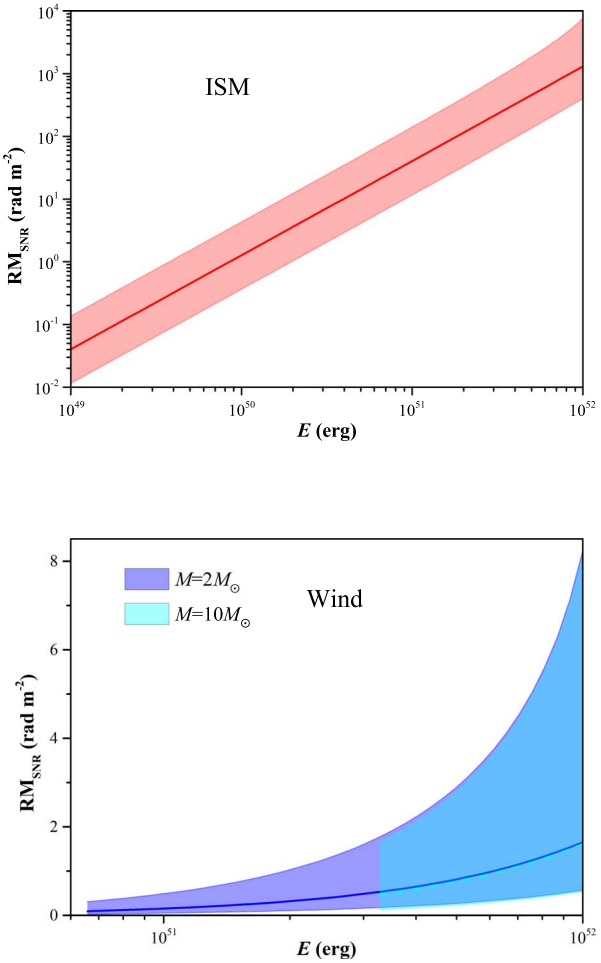

Figure 3. RM_{SNR} vs. energy of explosion E in ISM (upper panel) and wind (lower panel) environments. The lines are the same as those in Figure 1.

down as, along with the RM_{SNR} in the Sedov–Taylor phase ($t < t_{SP}$) (see Piro & Gaensler 2018),

$$\mathrm{RM_{SNR}} \simeq \begin{cases} 1.28 \times 10^5 \ \mathrm{rad\ m^{-2}} & \epsilon_{-1}^{1/2} t_3^{-1/5} E_{51}^{2/5} n_2^{11/10}, \\ t < t_{\rm SP} & \\ 4.94 \times 10^4 \ \mathrm{rad\ m^{-2}} & \epsilon_{-1}^{1/2} t_4^{-3/7} E_{51}^{0.67} n_2^{0.424}, \\ t > t_{\rm SP}. & \end{cases} \quad (14)$$

Combining with the relation between the energy of the SN explosion E and the number density n of ambient ISM in the top panel of Figure 1, one can derive RM_{SNR} as a power-law function of the explosion energy with an index 1.5, as displayed in the upper panel of Figure 3. It is also shown that RM_{SNR} can increase up to 10^4 rad m^{-2} when E approaches to 10^{52} erg.

Wind Scenario. The RM_{SNR} in a wind environment is calculated by (Piro & Gaensler 2018)

$$\mathrm{RM_{SNR}} \simeq \begin{cases} 0.002 \ \mathrm{rad\ m^{-2}} & x_{0.1} R_{*,2} B_{*,0} \mu_e^{-1} E_{51}^{-1} M_1 t_3^{-2}, \\ t < t_{\rm ch} & \\ 0.0017 \ \mathrm{rad\ m^{-2}} & x_{0.1} R_{*,2} B_{*,0} \mu_e^{-1} E_{51}^{-2/3} K_{13}^{5/3} t_4^{-4/3}, \\ t > t_{\rm ch} & \end{cases} \quad (15)$$

where $x \equiv v_{\rm rot}/v_{\rm w}$ ($v_{\rm rot}$ and $v_{\rm w}$ are the rotation velocity and wind velocity), $R_* = 100 R_\odot R_{*,2}$ and $B_* = 10^0 B_{*,0}$ G are the progenitor's radius and magnetic field, respectively. Fixing $x = 0.1$, $R_* = 100 R_\odot$, $\mu_e = 1$, and $B_* = 1$ G (even if they should be variable for different types of progenitors), and using the relation between the energy of the SN explosion E and the parameter K in the top panel of Figure 2 for different progenitors ($M = 2M_\odot$ or $M = 10M_\odot$), one gains a low $RM_{SNR} < 8$ rad m^{-2} when the explosion energy $E < 10^{52}$ erg, as exhibited in the lower panel of Figure 3.

Notice that there is both a foreground RM $= +223 \pm 2$ rad m^{-2} for SNR G57.2+0.8 (Kothes et al. 2018) and an RM $= +112.3$ rad m^{-2} for the highly polarized radio burst from SGR 1935+2154 (Zhang et al. 2020a). If this foreground RM has no contribution from the local environment of the SNR, it would indicate that $RM_{SNR} \sim -110$ rad m^{-2}, corresponding to an explosion energy $E \sim (1\text{–}5) \times 10^{51}$ erg in the ISM scenario from the upper panel of Figure 3.

5. Conclusions

In this Letter, we have utilized DMs contributed by the foreground ISM of our Galaxy and the local environments including the magnetar wind nebula and SNR to estimate the distance of SGR 1935+2154 potentially hosted in SNR G57.2+0.8, by assuming that the SGR and the SNR are indeed associated and combining with other observational constraints. The RM estimate and relevant results have been also discussed. Some interesting results are summarized as follows:

1. In the constant ISM scenario for the SNR, the energy of the SN explosion E is described by a power-law function as a function of the ambient medium density n with an index 1.0. Moreover, the distance, SNR radius, and DM contribution by the SNR are $D \simeq 6.5\text{–}11.5$ kpc, $R_{\rm SNR} \simeq 10\text{–}18$ pc, and $\mathrm{DM_{SNR}} \simeq 0\text{–}18$ pc $\mathrm{cm^{-3}}$ within a typical range of the explosion energy, respectively.
2. In the wind scenario for the SNR, the distance, SNR radius, and DM_{SNR} also spread over similar ranges of those in the ISM scenario for different mass of the SN ejecta.
3. For the RM estimate, the polarization observations from the radio burst of the SGR and the intensity maps of the SNR might signify that the RM contribution by the local environment of the SNR is about -110 rad m^{-2} with respect to the explosion energy $\sim(1\text{–}5) \times 10^{51}$ erg in the ISM scenario for the SNR.

Overall, our results relevant to the distance estimate are basically in agreement with the previous studies.

We would like to thank the referee for the very careful and helpful comments and suggestions that have allowed us to improve the presentation of this manuscript significantly. We also thank Wei-Li Lin and Yuan-Pei Yang for their helpful comments and discussions. This work was supported by the National Key Research and Development Program of China (grant No. 2017YFA0402600) and the National Natural Science Foundation of China (grant No. 11833003). C.M.D. is supported by the China Postdoctoral Science Foundation (No. 2020M671876) and the Fundamental Research Funds for the Central Universities (No. WK2030000019).

ORCID iDs

Shu-Qing Zhong https://orcid.org/0000-0002-1766-6947
Zi-Gao Dai https://orcid.org/0000-0002-7835-8585
Hai-Ming Zhang https://orcid.org/0000-0001-6863-5369
Can-Min Deng https://orcid.org/0000-0003-0471-365X

References

Bochenek, C. D., Ravi, V., Belov, K. V., et al. 2019, arXiv:2005.10828
Cao, X.-F., Yu, Y.-W., & Dai, Z.-G. 2017, ApJL, 839, L20
Cordes, J. M., & Lazio, T. J. W. 2002, arXiv:astro-ph/0207156
Cordes, J. M., & Lazio, T. J. W. 2003, arXiv:astro-ph/0301598
Draine, B. T. 2011, Physics of the Interstellar and Intergalactic Medium (Princeton, NJ: Princeton Univ. Press)
Gaensler, B. M. 2014, GCN, 16533, 1
Han, J. L., & Qiao, G. J. 1994, A&A, 288, 759
Israel, G. L., Esposito, P., Rea, N., et al. 2016, MNRAS, 457, 3448
Jansson, R., Farrar, G. R., Waelkens, A. H., & Enßlin, T. A. 2009, JCAP, 2009, 021
Kothes, R., Sun, X., Gaensler, B., & Reich, W. 2018, ApJ, 852, 54
Kozlova, A. V., Israel, G. L., Svinkin, D. S., et al. 2016, MNRAS, 460, 2008
Li, C. K., Lin, L., Xiong, S. L., et al. 2020, arXiv:2005.11071
Lin, W.-L., & Dai, Z.-G. 2016, RAA, 16, 38
Lyman, J. D., Bersier, D., James, P. A., et al. 2016, MNRAS, 457, 328
Mereghetti, S., Savchenko, V., Ferrigno, C., et al. 2020, arXiv:2005.06335
Metzger, B. D., Berger, E., & Margalit, B. 2017, ApJ, 841, 14
Pavlović, M. Z., Urošević, D., Vukotić, B., Arbutina, B., & Göker, Ü D. 2013, ApJS, 204, 4
Pejcha, O., & Prieto, J. L. 2015, ApJ, 806, 225
Piro, A. L., & Gaensler, B. M. 2018, ApJ, 861, 150
Prouza, M., & Šmída, R. 2003, A&A, 410, 1
Pshirkov, M. S., Tinyakov, P. G., Kronberg, P. P., & Newton-McGee, K. J. 2011, ApJ, 738, 192
Ranasinghe, S., Leahy, D. A., & Tian, W. 2018, OPhyJ, 4, 1
Ridnaia, A., Svinkin, D., Frederiks, D., et al. 2020, arXiv:2005.11178
Sedov, L. I. 1959, Similarity and Dimensional Methods in Mechanics (New York: Academic Press)
Simard-Normandin, M., & Kronberg, P. P. 1980, ApJ, 242, 74
Stanev, T. 1997, ApJ, 479, 290
Sun, X.-H., & Reich, W. 2010, RAA, 10, 1287
Sun, X. H., Reich, W., Waelkens, A., & Enßlin, T. A. 2008, A&A, 477, 573
Surnis, M. P., Joshi, B. C., Maan, Y., et al. 2016, ApJ, 826, 184
Tavani, M., Casentini, C., Ursi, A., et al. 2020, arXiv:2005.12164
Taylor, G. 1950, RSPSA, 201, 159
The CHIME/FRB Collaboration, Andersen, B. C., et al. 2020, arXiv:2005.10324
Tinyakov, P. G., & Tkachev, I. I. 2002, APh, 18, 165
Yang, Y.-P., & Zhang, B. 2017, ApJ, 847, 22
Yao, J. M., Manchester, R. N., & Wang, N. 2017, ApJ, 835, 29
Yu, Y.-W. 2014, ApJ, 796, 93
Zhang, C. F., Jiang, J. C., Men, Y. P., et al. 2020a, ATel, 13699, 1
Zhang, S. N., Tuo, Y. L., Xiong, S. L., et al. 2020b, ATel, 13687, 1
Zhang, S. N., Xiong, S. L., Li, C. K., et al. 2020c, ATel, 13696, 1
Zhang, S. N., Zhang, B., & Lu, W. B. 2020d, ATel, 13692, 1
Zhou, P., Zhou, X., Chen, Y., et al. 2020, arXiv:2005.03517